

Antiphase Fermi-surface modulations accompanying displacement excitation in a parent compound of iron-based superconductors

Kozo Okazaki^{1,*}, Hakuto Suzuki², Takeshi Suzuki¹, Takashi Yamamoto¹, Takashi Someya¹,
Yu Ogawa¹, Masaru Okada¹, Masami Fujisawa¹, Teruto Kanai¹, Nobuhisa Ishii¹,

Jiro Itatani¹, Masamichi Nakajima³, Hiroshi Eisaki³, Atsushi Fujimori², and Shik Shin^{1,*}

¹*Institute for Solid State Physics (ISSP), University of Tokyo, Kashiwa, Chiba 277-8581, Japan*

²*Department of Physics, University of Tokyo, Bunkyo-ku, Tokyo 113-0033, Japan*

³*National Institute of Advanced Industrial Science and Technology (AIST), Tsukuba, Ibaraki 305-8568, Japan*

**To whom correspondence should be addressed. E-mail: okazaki@issp.u-tokyo.ac.jp; shin@issp.u-tokyo.ac.jp*

We investigate the transient electronic structure of BaFe₂As₂, a parent compound of iron-based superconductors, by time- and angle-resolved photoemission spectroscopy. In order to probe the entire Brillouin zone, we utilize extreme ultraviolet photons and observe photoemission intensity oscillation with the frequency of the A_{1g} phonon which is antiphase between the zone-centered hole Fermi surfaces (FSs) and zone-cornered electron FSs. We attribute the antiphase behavior to the warping in one of the zone-centered hole FSs accompanying the displacement of the pnictogen height, and find that this displacement is the same direction as that induced by substitution of P for As, where superconductivity is induced by a structural modification without carrier doping in this system.

Photo-irradiation to a material can trigger a phase change into crystallographically and/or electronically modulated structures. This phenomenon is known as photo-induced phase transition (PIPT) [1]. The observation of extremely efficient photochromism (bi-directional switching of molecular structures induced by photo-irradiation) in polydiacetylenes is a pioneering work of the discovery of PIPT [2], and emergence of the photo-induced ‘hidden’ insulating phase in manganese oxide [3] and photo-induced insulator-metal transition in vanadium dioxide [4] are known as typical examples of PIPT in strongly correlated materials.

Recently, it has been reported that photo-induced superconductivity is realized in cuprate superconductors and doped fullerene [5–7]. For 1/8-doped (La,Eu,Sr)CuO₄ (Eu-LSCO), where superconductivity is not observed in the equilibrium state, the Josephson plasma edge was observed by an optical pumping of mid-infrared pulse. This has been claimed as evidence for photo-induced superconductivity [5]. Another example is YBa₂Cu₃O_{6+x} (YBCO), which has two CuO₂ layers within a unit cell and in which, differently from LSCO, two Josephson plasma edges and the transverse Josephson plasma mode due to the intra-bilayer and inter-bilayer couplings are observed. Surprisingly, the signal of the Josephson plasma has been detected even at room temperature [6, 8].

A key mechanism for the photo-induced superconductivity has been ascribed to atomic displacements induced by anharmonic effects of strongly excited infrared active phonon modes. Lattice modulation corresponding to the A_g phonon has been confirmed by time-resolved X-ray diffraction (TRXRD) measurements using a free electron laser for YBCO [9, 10]. On the other hand, the observation of coherent phonon excitation indicates the existence of lattice modulations induced by optical pumping, since

coherent phonon modes are excited followed by the lattice modulations according to the displacive excitation of coherent phonons (DECP) mechanism [11]. It has been reported that the photo-induced superconductivity can also be realized with near-infrared pump of 1.5 eV rather than mid-infrared pump in (La,Ba)₂CuO₄ [12]. This may be related to the lattice modulations through the DECP mechanism.

One of the most prominent features of BaFe₂As₂ (Ba122), the parent compound of another high-T_c superconductor system, iron-based superconductors [13], is the emergence of superconductivity under various conditions; that is, hole doping by substitution of K for Ba [14], electron doping by substitutions of Co for Fe [15], and isovalent substitution of P for As [16], as well as under high pressure [17]. In the isovalent substitution and high-pressure studies, superconductivity can be induced by structural modifications without carrier doping. This leads to the idea that this material could be driven into a superconducting state by photo-irradiation. To this end, it is crucial to study the transient electronic structure after photo-irradiation.

In this Rapid Communication, we investigate the transient electronic structure of Ba122 by time- and angle-resolved photoemission spectroscopy (TARPES) to explore the possibility of photo-induced superconductivity in this system. An extreme ultraviolet laser from high harmonic generation is used to study both the hole and electron FSs, and we observe photoemission intensity oscillation after optical pumping, of which the frequency corresponds to the A_{1g} phonon. We also find that the intensity oscillation is antiphase between the hole and electron FSs. We attribute this antiphase behavior to the warping [18] in one of the hole FSs accompanying the displacement of the pnictogen height. Since the pnictogen height is known to be important for superconductivity

in iron-based superconductors [19] and the Ba122-based system shows superconductivity by the reduced pnictogen height [16], our observation should be important for the realization of photo-induced superconductivity in iron-based superconductors.

TARPES measurements were performed with a commercial extremely stable Ti:Sapphire regenerative amplifier system (Astrella, Coherent) with the center wavelength of 800 nm and pulse duration ~ 30 fs, which was used for the pump light, and a Scienta R4000 hemispherical electron analyzer. After taking a second harmonic (SH) via 0.2-mm-thick β -BaB₂O₄ (BBO), the SH light is focused to the static gas cell filled with Ar and the high harmonics are generated. We selected 9th harmonic of the SH ($h\nu = 27.9$ eV) for the probe light using a set of SiC/Mg multilayer mirrors [20]. The probe light was p -polarized. (A component vertical to the surface was contained in the electric field.) While the other experimental conditions were similar to our previous report [21], we succeeded in observing a clear intensity oscillation corresponding to the coherent phonon excitation because the pulse duration of the fundamental laser was shortened and the stability was improved. The temporal resolution was evaluated to be ~ 80 fs from the TARPES intensity far above the Fermi level corresponding to the cross correlation between pump and probe pulses. The total energy resolution was set to ~ 250 meV. All the spectra were taken at 10 K. High quality single crystals of BaFe₂As₂ were grown by self-flux method and clean surfaces were obtained by cleaving *in situ*. Band structure calculations based on density functional theory (DFT) were performed using a WIEN2k package [22]. $a = 3.9625$ Å, $c = 13.0168$ Å, and $h = 1.3602$ Å [14] were used for the lattice parameters in equilibrium.

Figure 1(a) shows FS mapping measured with a He discharge lamp around the center and corner of the two-dimensional Brillouin zone (BZ), where the hole Fermi surfaces and electron FSs exist, respectively. The calculated FSs based on DFT are also overlaid. Figures 1(b) and 1(c) show the momentum integrated TARPES intensity measured across the hole and electron FSs, respectively, as a function of energy relative to the Fermi level (E_F) and pump-probe delay time. The integrated momentum regions of the hole and electron FSs are indicated by thick red and blue lines in Fig. 1(a), respectively. The spectra show that electrons are excited to above E_F upon photo-irradiation and relaxed after that. In addition, oscillatory behaviors can be recognized for the intensity above E_F in the spectra. This can be more clearly recognized in Figs. 1(d) and 1(e), where the integrated intensities of the regions surrounded by boxes in Figs. 1(b) and 1(c), respectively, are plotted. The dashed lines indicate the relaxation curves composed of an exponential decay function plus a residual slowly decaying component convoluted with a Gaussian corresponding to the temporal resolution. Now, the oscillatory compo-

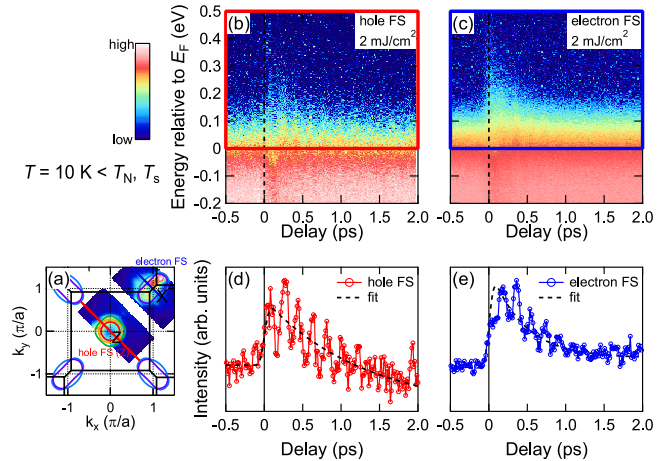


FIG. 1: Time-resolved ARPES (TARPES) spectra of BaFe₂As₂. (a) FS mapping measured with a He discharge lamp. The integrated momentum regions for the TARPES spectra across the hole and electron FSs shown in (b) and (c) are indicated by thick red and blue lines, respectively. The calculated FSs based on DFT are also overlaid. (b), (c) TARPES intensity images taken with the pump fluence of 2 mJ/cm² with respect to energy relative to E_F and pump-probe delay (b) around the zone center and (c) around the zone corner in the two-dimensional BZ, respectively. (d), (e) Integrated intensity from E_F to 0.5 eV above E_F of spectra shown in (b) and (c), respectively. T , T_N , and T_s are the measurement, Néel, and structural transition temperatures, respectively ($T_N \approx T_s = 142$ K).

nents are clearly seen as being superimposed onto the background relaxation curve.

To gain further insight into the observed oscillatory behaviors, we show in Fig. 2(a) the differential curves between the integrated intensities and relaxation curves indicated by the dashed lines in Figs. 1(d) and 1(e), and their fast Fourier transform (FFT) in Fig. 2(b). The peak positions are located at ~ 5.5 THz both for the hole and electron FSs, which evidences that the electronic system oscillates collectively with the frequency of the A_{1g} phonon, as reported by the previous studies [23–26]. By comparing the top and bottom positions of the oscillatory components between the hole and electron FSs, it is noticed that their oscillatory behaviors are antiphase contrary to the previous report [27–29]. In order to confirm this, we have fitted the oscillatory components to the damped oscillation function;

$$(Ae^{-(t-t_0)/\tau} + B) \cos \omega(t - t_0),$$

where t is the pump-probe delay time and ω is the frequency of the A_{1g} phonon ($= 5.5$ THz), and the others are fitting parameters. The fitting results are shown in Figs. 2(c) and 2(d) for the hole and electron FSs, respectively, and the obtained values are $A = -0.22$, $B = 0$, $\tau = 1.3$ ps, and $t_0 = -10$ fs for the hole FSs and $A = 0.32$,

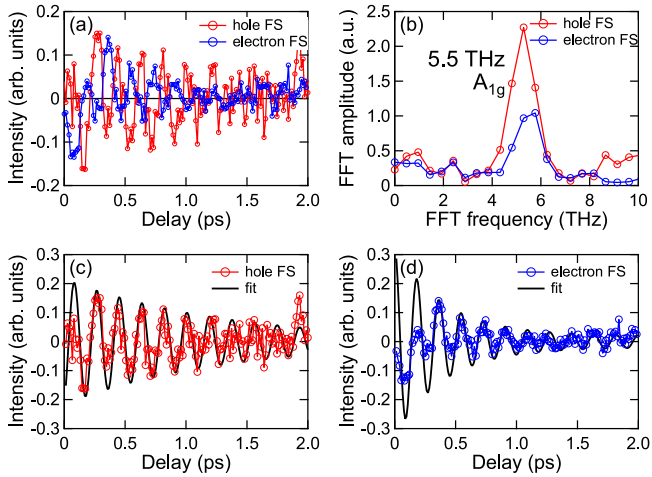


FIG. 2: Analysis of the oscillatory components of the ARPES spectra. (a) Oscillatory components of the hole and electron FSs deduced from the difference between the integrated intensities and decay functions shown in Figs. 1(d) and 1(e), respectively. (b) FFT amplitudes of the oscillatory components of the hole and electron FSs. (c), (d) Fitting results for the oscillatory components to the damped oscillator. Note that the phase of the oscillation is fully inverted between the hole and electron FSs.

$B = 0.02$, $\tau = 0.4$ ps, and $t_0 = 0$ fs for the electron FSs. From the facts that the sign of A is opposite between the hole and electron FSs and t_0 is much smaller than the temporal resolution, we concluded that the phase of the oscillation is fully inverted with respect to each other.

In order to investigate the origin of the phase inversion, we have performed band-structure calculations based on DFT for structures modulated by the A_{1g} phonon [31]. Because the A_{1g} phonon mode of Ba122 is the antiphase vibration of As atoms along the c axis, one can simulate the electronic structure modulated by the A_{1g} phonon mode with the modulation of the internal coordinate of the As atom z . We performed calculations for three values of z , where the pnictogen height h defined as the distance of As atoms from the nearest Fe layer is in equilibrium and varied by $\pm 5\%$ from the equilibrium value. The calculated hole FSs around the Γ and Z points are shown in Figs. 3(a)-3(c) and 3(d)-3(f), respectively, and the electron FSs around the X point are shown in Figs. 3(g) and 3(h) [32]. As can be recognized from the band dispersions, the most strongly modulated FS is the hole FS around the Z point contributed from the d_{z^2} orbital; that is, the d_{z^2} FS is strongly warped for the lower h value whereas the warping is dramatically weakened for the higher h value. As for the other two hole FSs, the modulation of the hole FS contributed from the $d_{yz/zx}$ orbital is relatively weak, while the d_{xy} hole FS has a significant modulation. According to the calculation of the photoemission matrix element, the matrix element of the d_{xy} orbital is smaller for the energy of probe light ($= 27.9$

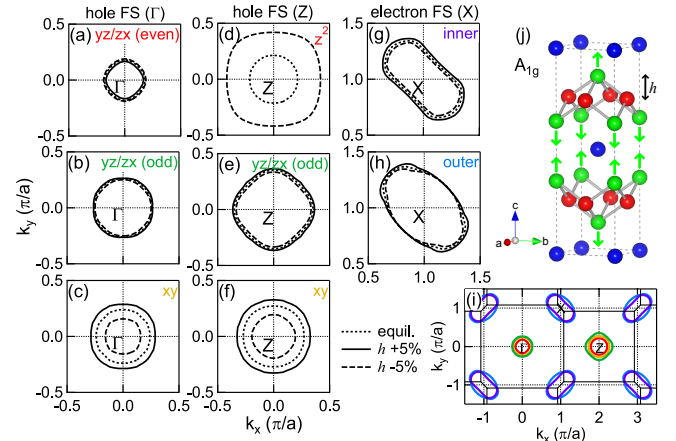


FIG. 3: Modulation of the electronic structure caused by the atomic displacement corresponding to the A_{1g} phonon. (a)-(c), (d)-(f) Modulations of the hole FSs around the Γ and Z points, respectively. (g), (h) Modulations of the electron FSs around the X point. (i) Calculated FSs of the equilibrium state shown in the extended two-dimensional BZ including the Γ , Z , and X points. (j) Crystal structure of BaFe₂As₂ and the definition of the pnictogen height h . Thick arrows indicate the displacements of the As atoms corresponding to the A_{1g} phonon. Note that the d_{xy} FS have low intensity due to matrix-element effects and will not be clearly visible by ARPES [30].

eV) due to the small emission angle of photoelectrons and the d_{z^2} orbital is more sensitive to p -polarization than other orbitals [30]. Thus, contribution from the d_{z^2} orbital is dominant for the temporal evolution of the ARPES intensity observed in Fig. 1(b). On the other hand, the modulations of the electron FSs are inverted with respect to that of the d_{z^2} hole FS, though their changes are slightly smaller; that is, they become larger for higher h and smaller for lower h . Thus, the observed antiphase oscillations between the hole and electron FSs are attributed to the FS modulations induced by the displacement of As atoms accompanying the A_{1g} coherent phonon excitation [33].

The mechanism of the coherent phonon excitation has been often discussed and the DECP mechanism is one of the most likely explanations [11]. In this mechanism, the adiabatic energy potential is modified due to photoexcitations and has the minimum with the finite atomic displacement corresponding to the A_{1g} phonon. As a result, the A_{1g} phonon is excited instantaneously and coherently. This mechanism has two important predictions that the oscillation of the coherent phonon shows $\cos(\omega t)$ dependence and only those modes with A_g symmetry are excited [11]. All the above features are consistent with our observations as shown in Fig. 2.

It should be worthwhile discussing possible temporally emerging electronic states. Figure 4 schematically describes the observed coherent phonon excitation and cor-

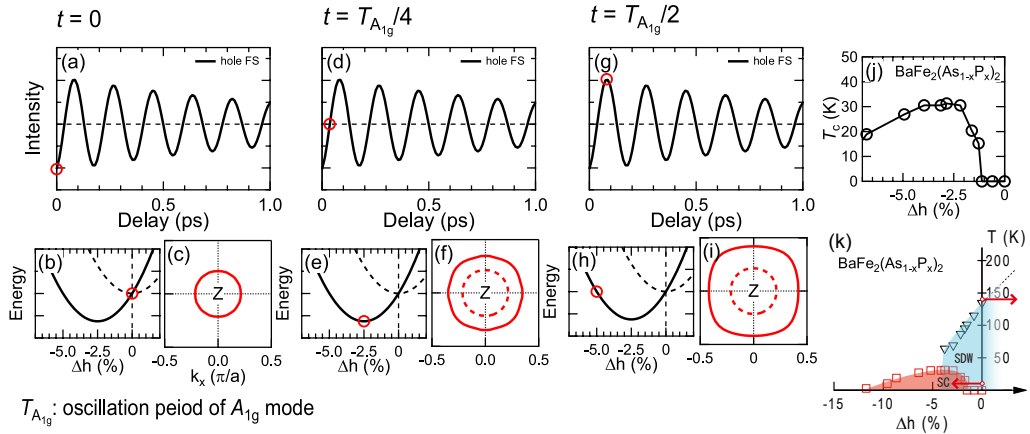


FIG. 4: Schematic description of the observed coherent phonon excitation and corresponding modulations of the d_{z^2} hole FS. (a)-(c) Oscillatory component of the TARPES intensity for the hole FSs (I_{osc}), the variation of the pnictogen height Δh , and the calculated d_{z^2} FS, respectively, at $t = 0$. The dashed and solid lines in (b) indicate the adiabatic energy potential at the equilibrium state and the state after the coherent phonon excitation. At $t = 0$, I_{osc} is negative, $\Delta h = 0$, and thus h is the largest and the size of the d_{z^2} FS around the Z point becomes the smallest. (d)-(f) The same as (a)-(c) but at $t = T_{A_{1g}}/4$, where $T_{A_{1g}}$ is the oscillation period of the A_{1g} phonon. At $t = T_{A_{1g}}/4$, I_{osc} is neutral, Δh is located where the energy is minimum, and the d_{z^2} FS has a medium size. (g)-(i) The same as (a)-(c) but at $t = T_{A_{1g}}/2$. At $t = T_{A_{1g}}/2$, I_{osc} is positive, Δh is negative and located where the energy is the same as that of $\Delta h = 0$, and the d_{z^2} FS around the Z point becomes the largest. The calculated d_{z^2} FS at the equilibrium state is also shown as dashed lines in (f) and (i) for comparison. If this potential modulation that induces the coherent phonon excitation persists for some time, it is expected that the pnictogen atoms are relaxed to the negative Δh positions and the warping of the d_{z^2} FS remains enhanced. (j) T_c of $\text{BaFe}_2(\text{As}_{1-x}\text{P}_x)_2$ plotted as a function of variation of the pnictogen height Δh . In $\text{BaFe}_2(\text{As}_{1-x}\text{P}_x)_2$, the pnictogen height lowers as P is substituted for As, and superconductivity emerges at $\Delta h \sim -1.3\%$ ($x \sim 0.16$). (k) Phase diagram of $\text{BaFe}_2(\text{As}_{1-x}\text{P}_x)_2$ with respect to T and Δh . The signs of Δh from TARPES and TRXRD are indicated by red arrows. The transition temperatures were taken from Ref. 16.

responding modulations of the d_{z^2} hole FS based on the DECP mechanism. As shown in Figs. 2(c) and 2(d), the oscillatory component of the TARPES intensity increases for the hole FSs, whereas that of the electron FSs decreases just after the arrival of the pump light. Correspondingly, the size of hole and electron FSs should increase and decrease, respectively, which results from the lowering of the pnictogen height. According to the DECP mechanism, the adiabatic potential after photo-excitation is modified such that it has a minimum at a smaller h . Here, in order to show the variation of the FS size more clearly, we assume the range of the variation of the pnictogen height Δh down to -5% . This Δh corresponds to the lowering of the pnictogen height by 6.8 pm and the variation of the Fe-As-Fe bond angle by 2.6° . This variation is too large compared to the observed amplitude of the lattice modulation by TRXRD measurements [25, 26]. However, as shown in Fig. 4(j), Ba122 shows superconductivity by lowering the pnictogen height with $\Delta h \sim -1.3\%$, which corresponds to the lowering of the pnictogen height by 2.0 pm. Therefore, if the atomic displacements minimizing the adiabatic potential after photo-excitation could be larger than this value and the accompanying lattice modulations persisted after the photo-excited electrons were relaxed to a metastable state, the observed transient electronic states

with coherent phonon excitation may enter a photo-induced superconducting state. This can be expected for semimetals like iron-based superconductors, because it has been known that the lifetime of photo-excited carriers in indirect-gap semiconductors like Si is far longer than the time scale of cooling dynamics [34, 35], whereas they are comparable in direct-gap semiconductors like GaAs [36]. Whether the photo-induced superconducting state can be realized in Ba122, it has to be confirmed by terahertz time domain spectroscopy or TARPES measurements with higher energy resolution in the future. Finally, we should note that the sign of the variation of the pnictogen height deduced here is opposite to that deduced from TRXRD measurements [25, 26]. This is probably because our measurements were performed at 10 K, far below the structural transition temperature (T_s), whereas the TRXRD measurements for the observation of the A_{1g} coherent phonon excitation were performed above T_s as schematically shown in Fig. 4(k) [37]. In addition, the difference of the probing depth between TRXRD and TARPES may also be a reason for this opposite tendency.

In conclusion, we have performed TARPES measurements on a parent compound of iron-based superconductors, BaFe_2As_2 , using an extreme ultraviolet laser from high harmonic generation. The antiphase photoemission

intensity oscillation between the hole and electron FSs was observed and attributed to the warping in the d_{z^2} FS around the Z point. We conclude that this displacement is the same direction as that induced by substitution of P for As, where superconductivity is induced by a structural modification without carrier doping. We also suggested a longer lifetime of the photo-excited state in semimetals like iron-based superconductors.

We would like to thank T. Tohyama, and M. Imada for valuable discussions and comments, and T. Yoshida for valuable comments. This work was supported by JSPS KAKENHI (Grant No. JP25220707 and JP26610095) and Photon and Quantum Basic Research Coordinated Development Program from the Ministry of Education, Culture, Sports, Science and Technology, Japan. H.S., T.S., and M.O. acknowledge the JSPS Research Fellowship for Young Scientists, and H.S. acknowledges Advanced Leading Graduate Course for Photon Science (ALPS) for financial supports.

-
- [1] Y. Tokura, *J. Phys. Soc. Jpn.* **75**, 011001 (2006), <http://dx.doi.org/10.1143/JPSJ.75.011001>.
- [2] S. Koshihara, Y. Tokura, K. Takeda, and T. Koda, *Phys. Rev. Lett.* **68**, 1148 (1992).
- [3] H. Ichikawa, S. Nozawa, T. Sato, A. Tomita, K. Ichiyangi, M. Chollet, L. Guerin, N. Dean, A. Cavalleri, S.-i. Adachi, T.-h. Arima, H. Sawa, Y. Ogimoto, M. Nakamura, R. Tamaki, K. Miyano, and S.-y. Koshihara, *Nat. Mater.* **10**, 101 (2011).
- [4] A. Pashkin, C. Kübler, H. Ehrke, R. Lopez, A. Halabica, R. F. Haglund, R. Huber, and A. Leitenstorfer, *Phys. Rev. B* **83**, 195120 (2011).
- [5] D. Fausti, R. I. Tobey, N. Dean, S. Kaiser, A. Dienst, M. C. Hoffmann, S. Pyon, T. Takayama, H. Takagi, and A. Cavalleri, *Science* **331**, 189 (2011), <http://www.sciencemag.org/content/331/6014/189.full.pdf>.
- [6] W. Hu, S. Kaiser, D. Nicoletti, C. R. Hunt, I. Gierz, M. C. Hoffmann, M. Le Tacon, T. Loew, B. Keimer, and A. Cavalleri, *Nat Mater.* **13**, 705 (2014).
- [7] M. Mitran, A. Cantaluppi, D. Nicoletti, S. Kaiser, A. Perucchi, S. Lupi, P. Di Pietro, D. Pontiroli, M. Riccò, S. R. Clark, D. Jaksch, and A. Cavalleri, *Nature* **530**, 461 (2016).
- [8] S. Kaiser, C. R. Hunt, D. Nicoletti, W. Hu, I. Gierz, H. Y. Liu, M. Le Tacon, T. Loew, D. Haug, B. Keimer, and A. Cavalleri, *Phys. Rev. B* **89**, 184516 (2014).
- [9] R. Mankowsky, A. Subedi, M. Forst, S. O. Mariager, M. Chollet, H. T. Lemke, J. S. Robinson, J. M. Glownia, M. P. Minitti, A. Frano, M. Fechner, N. A. Spaldin, T. Loew, B. Keimer, A. Georges, and A. Cavalleri, *Nature* **516**, 71 (2014).
- [10] R. Mankowsky, M. Först, T. Loew, J. Porras, B. Keimer, and A. Cavalleri, *Phys. Rev. B* **91**, 094308 (2015).
- [11] H. J. Zeiger, J. Vidal, T. K. Cheng, E. P. Ippen, G. Dresselhaus, and M. S. Dresselhaus, *Phys. Rev. B* **45**, 768 (1992).
- [12] D. Nicoletti, E. Casandru, Y. Laplace, V. Khanna, C. R. Hunt, S. Kaiser, S. S. Dhesi, G. D. Gu, J. P. Hill, and A. Cavalleri, *Phys. Rev. B* **90**, 100503(R) (2014).
- [13] Y. Kamihara, T. Watanabe, M. Hirano, and H. Hosono, *J. Am. Chem. Soc.* **130**, 3296 (2008).
- [14] M. Rotter, M. Tegel, and D. Johrendt, *Phys. Rev. Lett.* **101**, 107006 (2008).
- [15] A. S. Sefat, R. Jin, M. A. McGuire, B. C. Sales, D. J. Singh, and D. Mandrus, *Phys. Rev. Lett.* **101**, 117004 (2008).
- [16] S. Kasahara, T. Shibauchi, K. Hashimoto, K. Ikada, S. Tonegawa, R. Okazaki, H. Shishido, H. Ikeda, H. Takeya, K. Hirata, T. Terashima, and Y. Matsuda, *Phys. Rev. B* **81**, 184519 (2010).
- [17] T. Yamazaki, N. Takeshita, R. Kobayashi, H. Fukazawa, Y. Kohori, K. Kihou, C.-H. Lee, H. Kito, A. Iyo, and H. Eisaki, *Phys. Rev. B* **81**, 224511 (2010).
- [18] T. Yoshida, I. Nishi, S. Ideta, A. Fujimori, M. Kubota, K. Ono, S. Kasahara, T. Shibauchi, T. Terashima, Y. Matsuda, H. Ikeda, and R. Arita, *Phys. Rev. Lett.* **106**, 117001 (2011).
- [19] K. Kuroki, H. Usui, S. Onari, R. Arita, and H. Aoki, *Phys. Rev. B* **79**, 224511 (2009).
- [20] K. Ishizaka, T. Kiss, T. Yamamoto, Y. Ishida, T. Saitoh, M. Matsunami, R. Eguchi, T. Ohtsuki, A. Kosuge, T. Kanai, M. Nohara, H. Takagi, S. Watanabe, and S. Shin, *Phys. Rev. B* **83**, 081104 (2011).
- [21] H. Suzuki, K. Okazaki, T. Yamamoto, T. Someya, M. Okada, K. Koshiishi, M. Fujisawa, T. Kanai, N. Ishii, M. Nakajima, H. Eisaki, K. Ono, H. Kumigashira, J. Itatani, A. Fujimori, and S. Shin, *Phys. Rev. B* **95**, 165112 (2017).
- [22] P. Blaha, K. Schwarz, G. K. H. Madsen, D. Kvasnicka, and J. Luitz, *WIEN2K, An Augmented Plane Wave + Local Orbitals Program for Calculating Crystal Properties* (Karlheinz Schwarz, Techn. Universität Wien, Austria, 2001).
- [23] B. Mansart, D. Boschetto, A. Savoia, F. Rullier-Albenque, A. Forget, D. Colson, A. Rousse, and M. Marsi, *Phys. Rev. B* **80**, 172504 (2009).
- [24] I. Avigo, R. Cortés, L. Rettig, S. Thirupathaiah, H. S. Jeevan, P. Gegenwart, T. Wolf, M. Ligges, M. Wolf, J. Fink, and U. Bovensiepen, *J. Phys.: Condens. Matter* **25**, 094003 (2013).
- [25] L. Rettig, S. O. Mariager, A. Ferrer, S. Grübel, J. A. Johnson, J. Rittmann, T. Wolf, S. L. Johnson, G. Ingold, P. Beaud, and U. Staub, *Phys. Rev. Lett.* **114**, 067402 (2015).
- [26] S. Gerber, K. W. Kim, Y. Zhang, D. Zhu, N. Plonka, M. Yi, G. L. Dakovski, D. Leuenberger, P. Kirchmann, R. G. Moore, M. Chollet, J. M. Glownia, Y. Feng, J.-S. Lee, A. Mehta, A. F. Kemper, T. Wolf, Y.-D. Chuang, Z. Hussain, C.-C. Kao, B. Moritz, Z.-X. Shen, T. P. Devereaux, and W.-S. Lee, *Nat. Commun.* **6**, (2015).
- [27] L. X. Yang, G. Rohde, T. Rohwer, A. Stange, K. Hanff, C. Sohrt, L. Rettig, R. Cortés, F. Chen, D. L. Feng, T. Wolf, B. Kamble, I. Eremin, T. Popmintchev, M. M. Murnane, H. C. Kapteyn, L. Kipp, J. Fink, M. Bauer, U. Bovensiepen, and K. Rossnagel, *Phys. Rev. Lett.* **112**, 207001 (2014).
- [28] See Supplemental Material at [URL will be inserted by publisher] for additional results and discussions.
- [29] We note that the difference of the probe photon energy and experimental configurations (sample orientation and

polarization of probe light) could be possible reasons for the difference between the present results and previous reports [28].

- [30] X.-P. Wang, P. Richard, Y.-B. Huang, H. Miao, L. Cevey, N. Xu, Y.-J. Sun, T. Qian, Y.-M. Xu, M. Shi, J.-P. Hu, X. Dai, and H. Ding, *Phys. Rev. B* **85**, 214518 (2012).
- [31] The DFT calculations were performed for the tetragonal phase although the ARPES measurements were performed at 10 K in the orthorhombic phase with the antiferromagnetic ordering. However, this should not affect the variation of the FS sizes for the modulated structures.
- [32] Band dispersions for the modulated structures are shown in Supplemental Material[28].
- [33] We note that while the probe photon energy of 27.9 eV does not exactly trace the Z point, we confirmed that this does not affect this conclusion based on the calculations for various k_z values [28].
- [34] R. B. Hammond and R. N. Silver, *Applied Physics Letters* **36**, 68 (1980), <http://dx.doi.org/10.1063/1.91277> .
- [35] T. Suzuki and R. Shimano, *Phys. Rev. B* **83**, 085207 (2011).
- [36] R. A. Kaindl, D. Hägele, M. A. Carnahan, and D. S. Chemla, *Phys. Rev. B* **79**, 045320 (2009).
- [37] The pnictogen height as well as the Fe-Fe distance are slightly different between the tetragonal and orthorhombic phases. This means that the Fe-As-Fe bond angle is also different between these two phases. This slight structural difference in the thermally equilibrium state could be a reason for the different tendency in the photo-excited state.

Supplemental Material

Evidence for intensity oscillation rather than chemical potential oscillation

In the previous report, it has been reported that the effective chemical potential oscillates *in phase* between the Γ and M points as a function of pump-probe delay time^{S1}, contrary to our observation of the antiphase oscillation. In this work, we have observed the oscillation of the photoemission intensity rather than the chemical potential. Figure S1 shows the temporal evolution of the integrated ARPES intensities on the electron FSs in different integration ranges and their oscillatory components. The stronger time-dependent modulation in our ARPES data than those of Ref. S1 allows us to perform a qualitative intensity analysis. Irrespective of the integration range, the phase of the oscillatory components does not change. This is strong evidence that the photoemission intensity itself oscillates rather than the chemical potential, because if the chemical potential oscillated, the whole spectra would be shifted accordingly and the oscillation for the photoemission intensity would be out of phase between the higher and lower energy side of a spectral peak. In the case of the iron-based superconductors, the peak position of the spectra is located just below E_F due to the existence of the Fermi cutoff. If the chemical potential oscillated, the phase of the oscillatory component should be inverted between the integration ranges of [0.0, 0.5] eV and [-0.5, 0.0] eV.

Band dispersions for the modulated structures

Figures S2(a) and S2(b) show the band dispersions calculated for three values of h , which are in equilibrium and varied by $\pm 5\%$. The modulation around the Z point is the most pronounced.

Modulations of hole FSs at various k_z values

While we attributed the antiphase behavior between the hole and electron FSs to the warping in the d_{z^2} FS, which is expected to be the strongest at the Z point, the probe energy of 27.9 eV does not exactly trace the Z point in the Brillouin zone. According to the previous reports^{S2,S3}, k_z traced by 27.9 eV photons is expected to be around the midpoint between the Γ and Z points. In order to assess this point to our conclusion, we calculated the FS modulations at various k_z values as shown in Fig. S3. Based on these calculations, we could confirm that the modulation of the $d_{yz/zx+z^2}$ hole FS (Whether the dominant contribution to this FS is $d_{yz/zx}$ or d_{z^2} orbital, it switches depending on k_z .) is antiphase with respect to those of the electron FSs for any k_z value, while the modulation is the smallest at the Γ point and the largest

at the Z point. In this regard, since k_z traced by 22.1 eV used for Ref. S1 is very close to the Γ point, this could be a possible reason for the difference from the present results.

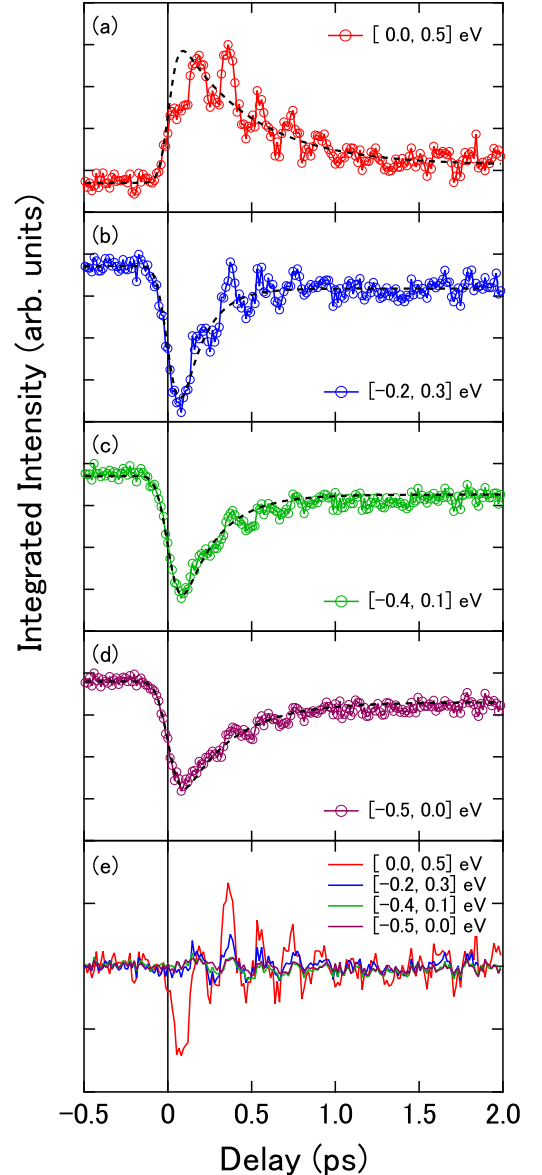


FIG. S1: Temporal evolution of the integrated photoemission intensities on the electron FS with various energy integration ranges and their oscillatory components. The integration ranges are (a) [0.0, 0.5] eV, (b) [-0.2, 0.3] eV, (c) [-0.4, 0.1] eV, and (d) [-0.5, 0.0] eV. The dashed lines indicate the decay function to extract the oscillatory components. (e) Deduced oscillatory components. Irrespective of the integration range, the phase of the oscillatory component does not change.

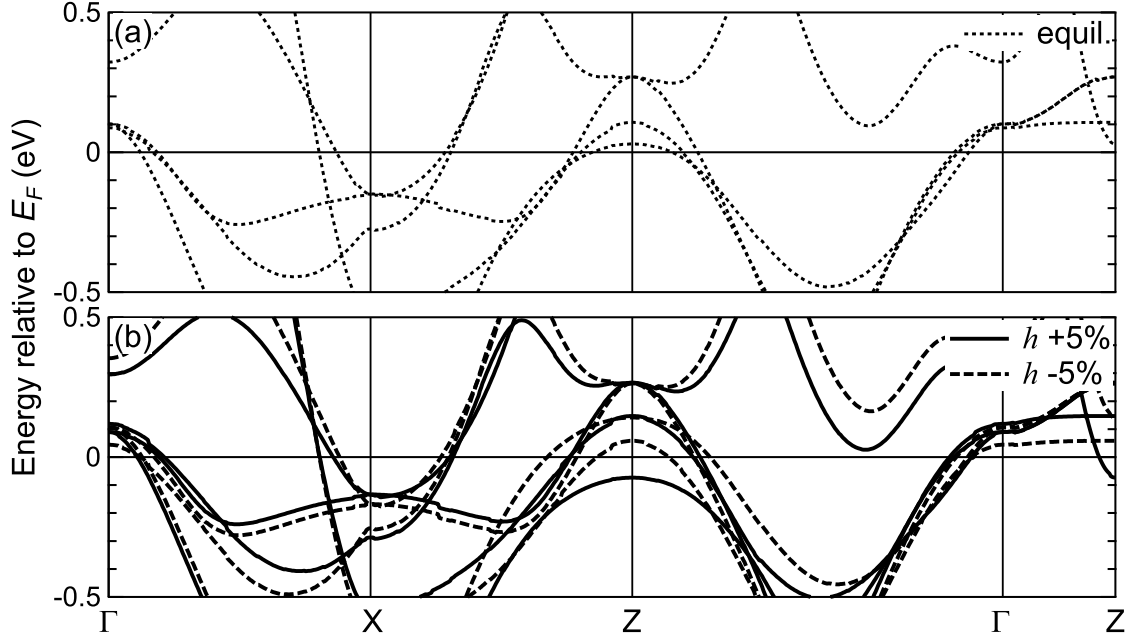


FIG. S2: Band dispersions of the modulated structures caused by the atomic displacement corresponding to the A_{1g} phonon. (a) Band dispersions of the equilibrium state. (b) Those of the modulated structures.

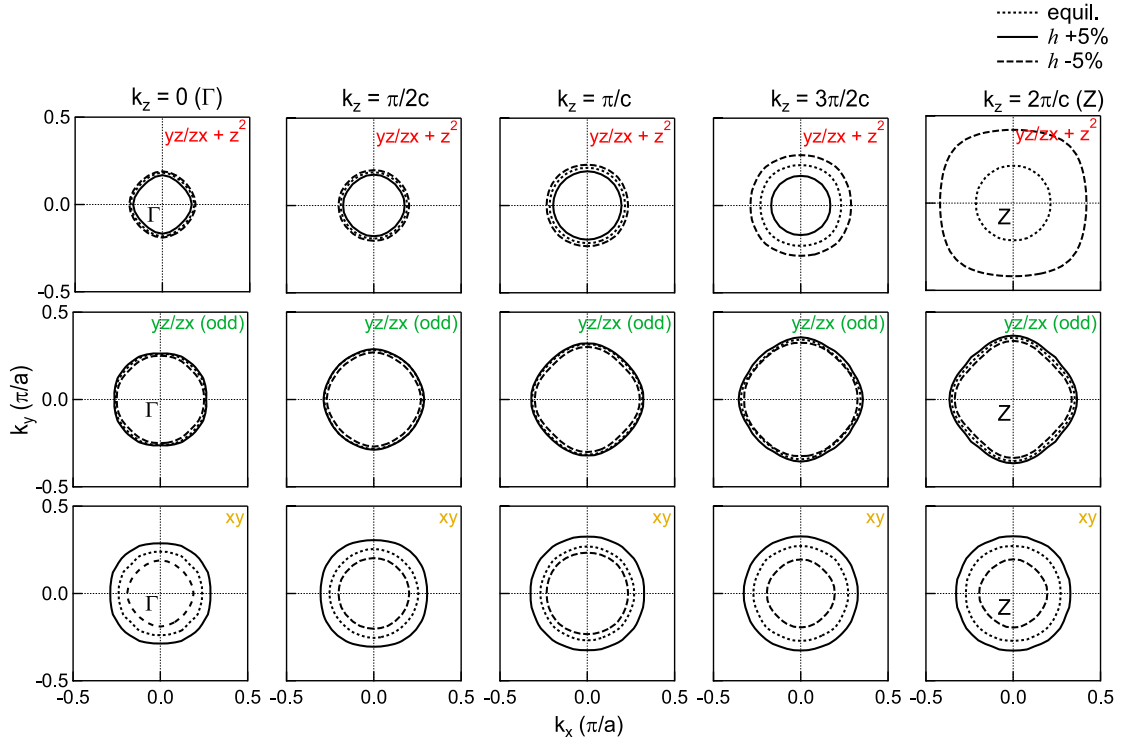


FIG. S3: Modulations of the hole FSs around the zone center at various k_z values. Notations are the same as those of Fig. 3(a)-3(f).

Animation of FS and structural modulations due to coherent phonon excitation

Supplemental Movie S1 includes an animation of FS and structural modulations due to the coherent excitation of A_{1g} phonon based on the DECP mechanism.

Movie S1: Animation of FS and structural modulations. In order to show the modulations more clearly, we assume the range of the variation of the pnictogen height Δh down to -10 %.

[S1] L. X. Yang, G. Rohde, T. Rohwer, A. Stange, K. Hanff, C. Sohrt, L. Rettig, R. Cortés, F. Chen, D. L. Feng, T. Wolf, B. Kamble, I. Eremin, T. Popmintchev, M. M. Murnane, H. C. Kapteyn, L. Kipp, J. Fink, M. Bauer, U. Bovensiepen, and K. Rossnagel, *Phys. Rev. Lett.* **112**, 207001 (2014).

[S2] T. Kondo, R. M. Fernandes, R. Khasanov, C. Liu, A. D.

Palczewski, N. Ni, M. Shi, A. Bostwick, E. Rotenberg, J. Schmalian, S. L. Bud'ko, P. C. Canfield, and A. Kaminski, *Phys. Rev. B* **81**, 060507 (2010).

[S3] G. Derondeau, J. Braun, H. Ebert, and J. Minár, *Phys. Rev. B* **93**, 144513 (2016).